OPTICA

Near-complete extraction of maximum stored energy from large-core fibers using coherent pulse stacking amplification of femtosecond pulses

Alexander Rainville,[1,*] Mathew Whittlesey,[1] Christopher Pasquale,[1] Yanwen Jing,[1] Mingshu Chen,[1] Siyun Chen,[1,2] Hanzhang Pei,[1] John Ruppe,[1] Tong Zhou,[1,2] Qiang Du,[3] Zhigang Zhang,[4] Guoqing Chang,[5] Franz X. Kärtner,[5] and Almantas Galvanauskas[1]

[1]Gérard Mourou Center for Ultrafast Optical Science, University of Michigan, 2200 Bonisteel Blvd., Ann Arbor, Michigan 48109, USA
[2]Current address: Lawrence Berkeley National Laboratory, One Cyclotron Road, Berkeley California 94720, USA
[3]Lawrence Berkeley National Laboratory, One Cyclotron Road, Berkeley, California 94720, USA
[4]State Key Laboratory of Advanced Optical Communication Systems and Networks, School of Electronics, Peking University, Beijing 100871, China
[5]Center for Free-Electron Laser Science, DESY, Notkestraße 85, 22607 Hamburg, Germany
*rainvila@umich.edu

Received 24 June 2024; revised 12 October 2024; accepted 14 October 2024; published 6 November 2024

High field science relies on ultrashort pulse lasers with multi-joule pulse energies for studying light–matter interactions under extreme conditions and for driving particle accelerators and secondary radiation sources of x rays, gamma rays, neutrons, positrons, muons, and protons. Next-generation laser drivers will require a 10^3-10^4 times increase in pulse repetition rates, producing multi-joule energies at multi-kilowatt average powers to enable practical applications in nuclear engineering, advanced materials, medicine, biology, homeland security, and high-energy physics. Spatially coherently combined femtosecond fiber lasers are recognized as a pathway to these next-generation drivers, with significant practical advantages including high efficiency and the possibility of compact integration. However, chirped pulse amplification in fibers is capable of extracting only a small fraction (usually ∼1%) of the maximum stored energy. Here we demonstrate near-complete maximum stored energy extraction with low accumulated nonlinearity from a large-core fiber amplifier using coherent pulse stacking amplification. We have amplified a 81-pulse stacking burst in a 85 μm core chirally coupled core Yb-doped fiber, extracting up to 9.5 mJ (∼90% of stored energy) with <4.5 radians of accumulated nonlinear phase, temporally combined this burst into a single pulse, and achieved 4.2 mJ pulses of 313 fs bandwidth-limited duration after compression. This represents, to our knowledge, the highest energy extracted and compressed into a femtosecond pulse from a single fiber amplifier, enabling approximately two orders of magnitude size reduction of future high-energy coherently spatially combined fiber laser arrays.

https://doi.org/10.1364/OPTICA.533803

1. INTRODUCTION

High field science has been enabled by the emergence of Ti:sapphire based chirped-pulse amplification (CPA) laser systems that produce 1–10 J high-energy sub-100-fs ultrashort pulses needed for driving laser wakefield acceleration (LWFA) [1,2], secondary radiation sources [1,3,4], and other intense laser–matter interactions [5]. However, practical applications and further development of high-field science are limited by the low (typically <1 Hz) repetition rates of these lasers. Potential high-impact applications in medicine, material science, high-energy physics, nuclear spectroscopy, and homeland security [1–8] require very high radiation fluxes and high-precision control of laser-target interactions, achievable only at laser pulse repetition rates of 1–100 kHz, far beyond the capability of current Ti:sapphire-based ultrafast laser technology.

New laser media promising to achieve CPA of ultrashort pulses at the required high repetition rate and high energy include Yb:YAG thin-disk [9], Tm:YLF solid-state [10], and Yb-doped fiber lasers [11], which have much higher pumping efficiency and significant thermal dissipation advantages over Ti:sapphire lasers. Among these new media, fiber lasers can provide the shortest duration pulses, can be compactly integrated into very robust systems, and have by far the highest efficiency, with wall-plug efficiencies of up to 50% reported for industrial 100 kW continuous-wave (CW) lasers [12,13]. Power and energy scaling in fiber lasers can be achieved through coherent beam combination (CBC) of multiple parallel amplifiers [14], which has been demonstrated at multi-kW average powers in both CW and ultrashort-pulse formats [15,16].

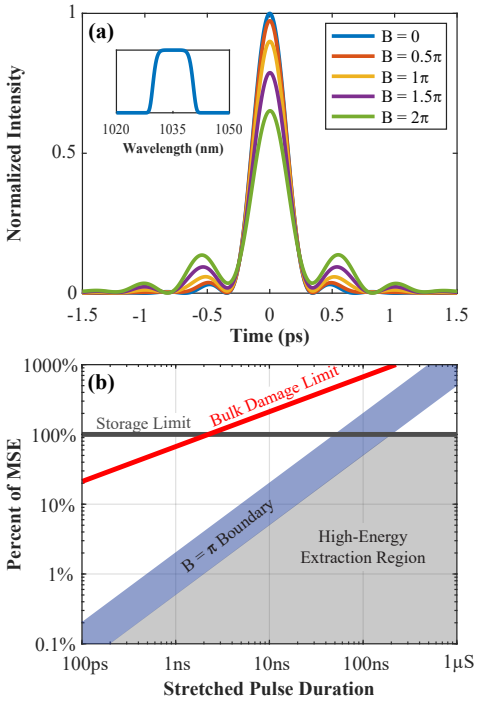

Fig. 1. Effects of nonlinear phase accrual in fiber CPA: (a) calculated compressed pulse traces for increasing levels of peak nonlinear phase accrued for a 10 nm FWHM spectrum (inset) and (b) calculated dependence of percent of maximum stored energy extracted on chirped pulse duration, with $B < \pi$ and bulk damage [18] boundaries shown.

CW fiber CBC systems with $\sim 10^2$ parallel channels are now the dominant technology for laser systems operating at >100 kW. However, due to very limited energies achievable per individual fiber CPA channel, ultrashort-pulse CBC array sizes will need to contain approximately 10^4-10^5 parallel amplifiers for reaching the 1–10 J range of pulse energies required by high-field science, approximately two to three orders of magnitude more channels than for current 100-kW-class CW systems.

Large array sizes result from the fact that Yb-doped fiber CPA is limited by nonlinear phase accrual to a few percent of the maximum stored energy in a fiber, on the order of a few hundred microjoules for state-of-the-art 80-85 μm large-core fibers [17]. When the accrued nonlinear phase, characterized by the B-integral [17], becomes too high, it distorts compressed pulses, lowering their peak power and adding pre- and post-pulse "wings." As an illustration, Fig. 1(a) shows the calculated effect of increasing B-integral on compressed pulse quality in a 300 fs bandwidth-limited CPA system assuming a flat top 1 ns stretched pulse. Since this is a strongly stretched pulse, its temporal shape is identical to its spectral shape [19] (shown in the inset). For $B \leq \pi$ the peak power remains above 90% of its bandwidth-limited maximum value and the energy content in pulse wings remains low. Although this calculation is sensitive to the spectral shape, in practice $B = \pi$ is a good approximate upper boundary for high-fidelity pulse compression.

The B-integral is proportional to the signal peak power and, therefore, for a fixed pulse energy, decreases with increasing pulse duration. Figure 1(b) shows how the pulse energy at the $B = \pi$ boundary depends on stretched pulse duration, normalized to the maximum stored energy (MSE) available in a fiber amplifier operating in the regime where the pulse repetition period is longer than the gain recovery time [20]. The normalized dependence calculated here for a signal at $\lambda \approx 1$ μm is universal, approximately independent from fiber doped-core area $A_{\text{dop.}}$ and length L, because both the B-integral and stored energy are proportional to each [see Supplement 1]. Only relatively minor fiber-to-fiber variations result from differences in doping concentrations as well as other factors [see Supplement 1]. This relatively minor variation is shown by representing the $B = \pi$ boundary as a band in Fig. 1. This figure immediately reveals that fiber CPA systems, where stretched pulse durations are constrained by compressor grating size to 1–3 ns, are limited to approximately 1%–3% of the MSE and that full extraction at low nonlinearity requires pulses longer than 60 ns. Amplification at the maximum stored energy limit can enable femtosecond pulses with up to 100 times higher energies from a fiber than are available when only using CPA.

It is important to emphasize the difference between the maximum stored energy and a stored energy under given operation conditions in an amplifier. The MSE represents the maximum achievable inversion in the amplifier, which is maintained only when the pulse repetition period is comparable or longer than the gain recovery time (see Supplement 1). When the pulse repetition period is shorter than the gain recovery time, the inversion (and thus the gain) does not fully recover between pulses, thus reducing stored energy to a fraction of the MSE. The gain recovery time decreases with increasing pumping (see Supplement 1), meaning that increasing pump power allows us to access MSE-level pulses at an increasing repetition rate.

In this paper we show that coherent pulse stacking amplification (CPSA) [21], a coherent time-domain pulse combining technique, enables femtosecond pulse amplification at the maximum stored energy limit with low accrued nonlinearity due to its ability to efficiently combine a strongly saturated pulse burst containing a large number of stretched pulses. We experimentally demonstrate pulse amplification of up to 9.5 mJ using an 81-pulse burst of ~1 ns long stretched pulses (i.e., an effectively 80 ns long signal), followed by coherent temporal combining of this burst into a single ~1 ns pulse and then its subsequent compression back to a bandwidth-limited duration of 313 fs. The highest energies achieved constitute ~90% of the maximum stored energy in the 85 μm core (65 μm MFD) Yb-doped chirally coupled core (CCC) [22] fibers used in these experiments. Previously reported high-energy femtosecond pulse amplification results using a divided-pulse amplification (DPA) technique based on 8-pulse combining with delay lines [23,24] reported much lower 3.3 mJ extraction at 20 kHz from a similar 62 μm mode-field diameter fiber power amplifier [25], indicating an operation regime with stored energies well below the MSE level.

We also show theoretically and experimentally that for amplification at the MSE level, it is essential to minimize nonlinear phase accrual by amplifying stacking bursts that have a specially crafted amplitude profile that produces equal nonlinearity for each pulse in the burst. These equal-nonlinearity burst profiles are characterized by a strong front-to-back amplitude variation and therefore require sufficient degrees of freedom in controlling the stacking burst and pulse combiner. We demonstrate that CPSA, which combines pulses using resonant Gires–Tournois interferometer (GTI) cavities, has enough degrees of freedom to efficiently combine equal-nonlinearity burst profiles with a large number of pulses, allowing amplification, temporal combination, and compression at the fiber maximum stored energy. This work opens a pathway towards 1–10 J coherently combined fiber laser systems with only 10^2-10^3 parallel amplifiers.

2. COHERENT PULSE STACKING AMPLIFICATION

A coherent pulse stacking amplification system consists of three major steps: (1) stacking burst formation, (2) pulse stretching and amplification, and (3) pulse stacking and compression. The stacking burst is formed directly from a high repetition rate $f_{\text{rep.}}$ mode-locked pulse train using a pair of fast amplitude and phase electro-optic modulators, which imprint individual amplitudes and phases on each femtosecond pulse in the burst. The burst is then transformed into a quasi-continuous long pulse by passing it through a pulse stretcher, where the dispersion is chosen to such that the stretched pulse duration is nearly the pulse repetition period $T_{\text{rep}} = f_{\text{rep.}}^{-1}$, after which the quasi-CW burst is amplified to high energies in an amplifier chain. After amplification, the burst is coherently stacked (i.e., temporally combined) into a single pulse using a set of GTI cavities and then compressed to femtosecond duration in a pulse compressor.

Details of coherent pulse stacking (CPS) using GTI cavities are presented elsewhere [26], but for the subsequent discussion it is instrumental to briefly summarize its operating principle. A GTI cavity is a ring cavity formed by a partially reflecting beamsplitter and two or more fully reflecting folding mirrors [27]. A GTI pulse stacker consists of a sequence of N ($N \geq 1$) such GTI cavities, where each ith cavity is characterized by a beamsplitter reflectivity R_i, a round-trip phase ϕ_i, and a round-trip period T_i. Each cavity round-trip period T_i is defined to be an integer multiple m_i of the pulse repetition period $T_{\text{rep.}}$ ($T_i = m_i \times T_{\text{rep.}}$), and the round-trip phase ϕ_i is defined as a fractional optical-cycle difference between this period T_i and the exact cavity round-trip T: $T - T_i = \phi_i/2\pi \times \lambda/c$, where λ is the optical wavelength of the signal and c is the light velocity. A GTI stacker is a linear time invariant system. Therefore, it is fully characterized by its impulse response, in this case the burst of pulses generated when a single pulse is incident into the stacker. Each pulse in the impulse response burst has phase and amplitude determined by the choice of N beamsplitter reflectivites' R and N cavity round-trip phases ϕ.

For a lossless stacker, inputting the time-reversed impulse response yields a single stacked pulse at the output (i.e., the initial impulse). Thus the time-reversed impulse response constitutes a stacking burst, comprising of two parts: (1) a main burst with a finite number of pulses M containing a majority of the energy and (2) a low-amplitude semi-infinite pre-burst containing at most a few percent of the overall energy. A properly shaped main burst is used for energy extraction, while the pre-burst can be truncated without appreciable effect on stacking efficiency; however, truncation reduces pre-pulse contrast in front of the stacked pulse. Inclusion of the pre-burst is necessary for maximizing this contrast through allowing fields to slowly build in the cavities before the main burst arrives.

A stacker is designed using a numerical optimization procedure that matches the calculated time-reversed impulse response to the desired stacking burst amplitude profile by varying each cavity phase ϕ_i and beamsplitter reflectivity R_i; however, a perfect match is not always possible. It is an essential feature of GTI-based coherent temporal pulse combining that a stacking burst can deviate significantly from an exact replica of the time-reversed impulse response and still provide a very high stacking efficiency. This means that GTI-based stacking is highly adaptable—once a stacker design is chosen, i.e., all R_i are chosen, the main burst amplitude profile can be varied over a wide range by controlling cavity phases ϕ_i and/or individual pulse phases in the stacking burst. Note that this does not necessarily lead to pre-pulse contrast degradation for the stacked pulse—we report elsewhere [26] that multiple stacking burst control strategies exist that simultaneously maintain high stacking efficiencies and high pre-pulse contrasts. The practical importance of this inherent-to-CPS adaptability is twofold: it significantly broadens the range of possible GTI stacker design options and it enables highly saturated energy extraction from an amplifier, which will be discussed in Section 3.

The number of pulses M in the main stacking burst depends on the stacker configuration. A great variety of stacker configurations are possible that accommodate nearly every different M, each configuration specified by the number of GTI cavities used N and the set of their round-trip durations $\{T_1, T_2, ..., T_N\}$. The simplest is an equal-length stacker configuration, where all round-trips are equal and matched to the pulse separation in the stacking burst $T_i = T_{\text{rep.}}$ for all i. The main advantage of an equal-length stacker configuration of N cavities is that the impulse response can be perfectly matched to any desired main-burst shape of $M \approx 2N$ pulses due to the availability of $2N$ independent design parameters of cavity phase and beamsplitter reflectivity. However, as full energy extraction requires main bursts with $M \sim 10^2$ pulses (see Fig. 1), this configuration would need an impractically large number of cavities.

This problem can be solved with multiplexed-length stacker configurations, using GTIs with different round-trip durations, each specified by a corresponding m_i. As an illustration, consider one such class of N-cavity stackers consisting of $N/2$ GTIs with short $m_i = 1$ round-trips, and of $N/2$ GTIs with long $m_i \approx N$ round-trips—a so-called "$N/2 + N/2$" configuration. Since each group can stack $\sim N$ pulses, but with the pulse-to-pulse separation $T_{\text{rep.}}$ for short-round-trip GTIs and the separation $\sim N \times T_{\text{rep.}}$ for long round-trip GTIs, the total number of pulses in the main stacking burst can be $(\sim N)^2$. However, due to the mismatch between the $\sim 2N$ cavity design parameters and the $(\sim N)^2$ number of main burst pulses, the main burst amplitude cannot be precisely matched to the impulse response. Nevertheless, the adaptability of coherent pulse stacking allows accommodation of the required stacking burst profiles, as illustrated in the following design example.

This work uses a 4 + 4 GTI multiplexed stacker designed to stack 81 pulses into one [26]. This design provides an effective burst length 81 ns (when pulse separation $f_{\text{rep.}}^{-1} = 1$ ns), long enough to extract full fiber energy at low nonlinearity. Multiplexing four cavities of $T_{\text{rt}} = 1$ ns (30 cm round-trip length) with four cavities of $T_{\text{rt}} = 9$ ns (2.7 m round-trip length) allows efficient combining of 81 pulses without using the 40 cavities that would be needed in the equal-length case. Figure 2(a) shows the design of this stacker, which is nested to reduce the footprint. The calculated stacked trace for a pre-burst truncated equal-amplitude input is shown in Fig. 2(b). The calculated stacking efficiency η_s (defined as the stacked pulse energy divided by the total stacked-waveform energy) for a pre-burst truncated input is 98.1% with 19.4 dB pre-pulse contrast; including the pre-burst increases the stacking efficiency to 99.4% with 27.1 dB pre-pulse contrast. The pre-pulse contrast is defined as the ratio between the peak powers of the largest pre-pulse and the stacked pulse.

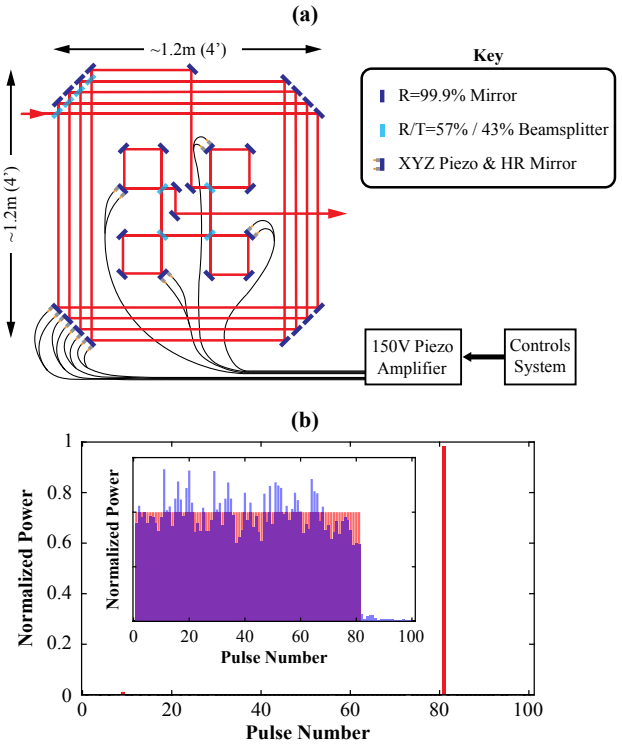

Fig. 2. Design of a 4 + 4 GTI stacker for 81 → 1 pulse stacking: (a) multiplexed-length GTI cavities, nested to reduce footprint, and (b) calculated equal-amplitude stacking-burst trace for a pre-burst truncated 81-pulse input, shown in red in the inset, and the calculated impulse response, shown in blue in the inset. Note that despite the deviation from the impulse response, the stacking efficiency is calculated to be 98.1% with 19.4 dB pre-pulse contrast.

3. STACKING BURST PROFILES FOR LOW NONLINEARITY EXTRACTION APPROACHING THE MAXIMUM STORED ENERGY LIMIT

The principal advantage of the CPSA technique is adaptability that allows preservation of high stacking efficiencies even for highly amplitude shaped stacking bursts from a strongly saturated amplifier. Such reshaping is caused by the amplifier population inversion depleting along the pulse burst. As a result, the highest gain occurs at the burst's leading edge, usually producing a temporally decaying burst profile with the decay increasing as saturation increases for higher pulse energies. Although in general saturation-induced gain variation is wavelength dependent, spectral reshaping effects are negligible for sufficiently narrow-bandwidth signals, such as ∼10 nm used in this work. Analysis in this monochromatic-approximation limit can ignore saturation-induced reshaping within each stretched pulse in the burst.

This saturation-induced decrease in gain would lead to increasing accrual of B-integral along the amplified stacking burst consisting of pulses with equal amplitudes. However, the decreasing profile of a strongly saturated amplified burst mitigates this effect and, as we show next, can be precision tailored to produce a B-integral precisely equal for all pulses in the burst. Because the first pulse accrues the lowest B-integral, such tailoring automatically minimizes the accumulated nonlinear phase for the whole burst. The amplified output burst shape can be controlled through shaping of the input burst. Since the required equal-nonlinearity burst shape varies with degree of saturation, it is important that such control be implemented electronically to accommodate varying amplification conditions in a running laser system.

Equal-nonlinearity stacking profiles within the monochromatic approximation can be found analytically [28] using the Frantz–Nodvik equations [29] for saturated energy amplification. For reference, we provide the analytical derivation in the Supplement 1, which reveals that equal-nonlinearity burst shape solutions are achievable even at the MSE level and shows how their general decaying-amplitude shapes change under varying saturation conditions.

However, this analytical approximation is derived assuming exponential gain along the fiber amplifier, which is a significant oversimplification and inaccurate for high saturation conditions. Therefore, precise calculation requires a numerical model in which the input pulse burst $P_{\text{in}}(t)$ propagates along z encountering the actual amplifier inversion profile $\Delta N(z, t)$. The calculation can be done in two separate steps: (1) calculate the inversion profile $\Delta N(z)$ in steady-state conditions under CW pumping, accounting for amplified spontaneous emission (ASE), and (2) propagate the pulse burst through the inversion using rate equations [30,31]. The calculated B-integral for every pulse in the burst can be equalized through a simple optimization method. Here we use this model under the monochromatic approximation; however, the approach is fully valid for modeling the burst as individual chirped pulses, each with their own shape and spectrum. For this calculation circular polarization is assumed, which reduces the value of n_{2I} by 2/3 with respect to the typically measured linear polarization value.

Figure 3 shows the numerically calculated equal-nonlinearity pulse bursts at increasing saturation (solid lines) and the analytically calculated result at 10 mJ (dashed line), along with the calculated nonlinear phase, for the 1.8-m-long 85-μm-core CCC fiber amplifiers discussed in the next section. The peak powers and phases of each individual pulse are represented as a smooth curve for clarity. We can clearly see that the analytical solution confirms that a decreasing amplitude profile can be used to equalize pulse burst B-integral and also that the assumption of pulse peak power exponential growth inaccurately calculates $P(t)$ and underestimates the accrued nonlinear phase. The numerical model properly accounts for saturation effects, increasing the fraction of energy at the front of the pulse burst (where gain is near exponential) to match the B-integral of the heavily saturated pulses at the end of the burst. The 10 mJ pulse burst corresponds to ∼90% energy extraction (measurement described in next section), indicating a near-complete maximum stored energy extraction at low nonlinearity (B-integral is slightly above π) with ∼81 ns burst length,

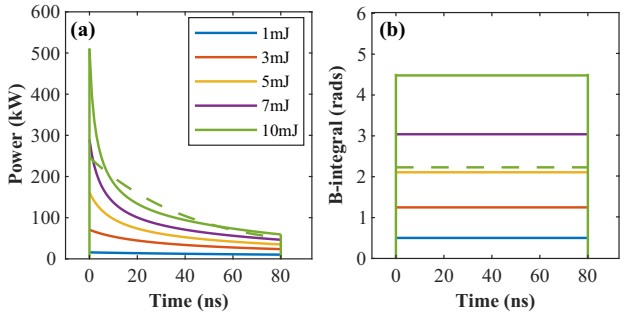

Fig. 3. Numerically calculated equal nonlinearity bursts for several different amplifier output energy levels and the corresponding optimized phase profile. The dashed line shows a comparison to the analytical equal-nonlinearity theory.

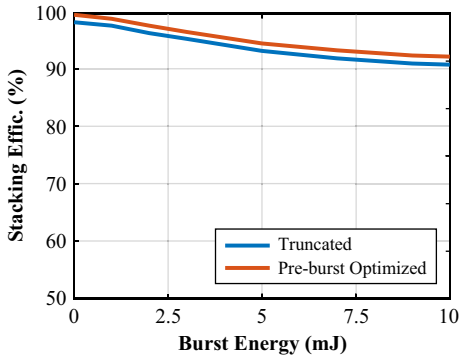

Fig. 4. Calculated stacking efficiency for the truncated bursts shown in Fig. 3 as well as an optimized burst that includes pre-pulses.

consistent with Fig. 1. The stacking efficiency η_s of the equal-nonlinearity bursts calculated for both the truncated and pre-burst optimized cases is shown in Fig. 4, indicating stacking efficiencies above 90% even for the 10 mJ bursts.

4. EXPERIMENTAL DEMONSTRATION OF FEMTOSECOND CPSA OPERATING CLOSE TO THE MAXIMUM STORED ENERGY LIMIT

The setup for experimental validation is shown in Fig. 5. The 81 pulse stacking burst is generated by amplitude and phase modulating successive pulses from a 1 GHz fiber oscillator [32] using fiber-coupled 10 GHz electro-optic modulators (EOMs), after which the pulses are stretched to 900 ps by a Martinez stretcher yielding ∼81 ns long burst. After pulse stretching the burst rep-rate is down-counted to 100 kHz by a fiber-coupled AOM. Single-mode fiber preamplifiers compensate loss after the EOMs, stretcher, and first AOM and increase burst energy to 1 μJ. Further amplification is done in a 25-μm-core large-mode area (LMA) fiber amplifier, after which a final AOM downcounts to the final rep-rate of 1–10 kHz. Burst energy is increased to 250 μJ by an ∼1 m long 85-μm-core CCC fiber pre-amplifier before entering the final stage of 1.8 m of 85-μm-core CCC fiber.

This CCC fiber is an all silica, effectively single-mode large-core fiber that can store more than 10 mJ depending on mode-field diameter and other parameters [22]. This is a double-clad fiber (cladding diameter 400 μm), with Yb-ion concentration in the 85 μm core of 5×10^{25} m^{-3}, providing ∼90% pump absorption after the 1.8 m at 976 nm. The measured mode-field diameter is 65 μm. We experimentally evaluated stored energy in this final-stage fiber amplifier by measuring small-signal gain and pulsed energy gain for varying degrees of saturation and fitting these results to the Frantz–Nodvik model of this fiber amplifier, as described in Supplement 1, Section 3. The maximum stored energy in this amplifier is measured to be 10.6 mJ, with a corresponding small signal gain of 46 dB, as shown in Fig. 6. With a 200 μJ seed up to 9.5 mJ can be extracted, corresponding to an extraction efficiency of 88%. All experiments reported in this work are performed at the pulse repetition rate of 2 kHz, too low for high average-power efficiency. However, the amplifier has been validated to store the same energies at up to 8 kHz repetition rate (limited by the available pump power), indicating that continuous-wave level efficiencies at the MSE level are achievable from this amplifier by simultaneously increasing the pulse repetition rate and pump power.

After amplification the high-energy pulse burst is temporally combined in the 4 + 4 GTI stacker described in Section 2 and then compressed. The beam into the GTI stacker is diffraction limited due to the effectively single mode operation of the CCC fiber (measured M-squared is 1.04). The GTI stacker alignment involves achieving highly accurate spatial and angular beam overlap, as well as round-trip timing in each cavity using specially developed and partially automated procedures described in [26]. The compressor maintains a high measured transmission of 84% due to the use

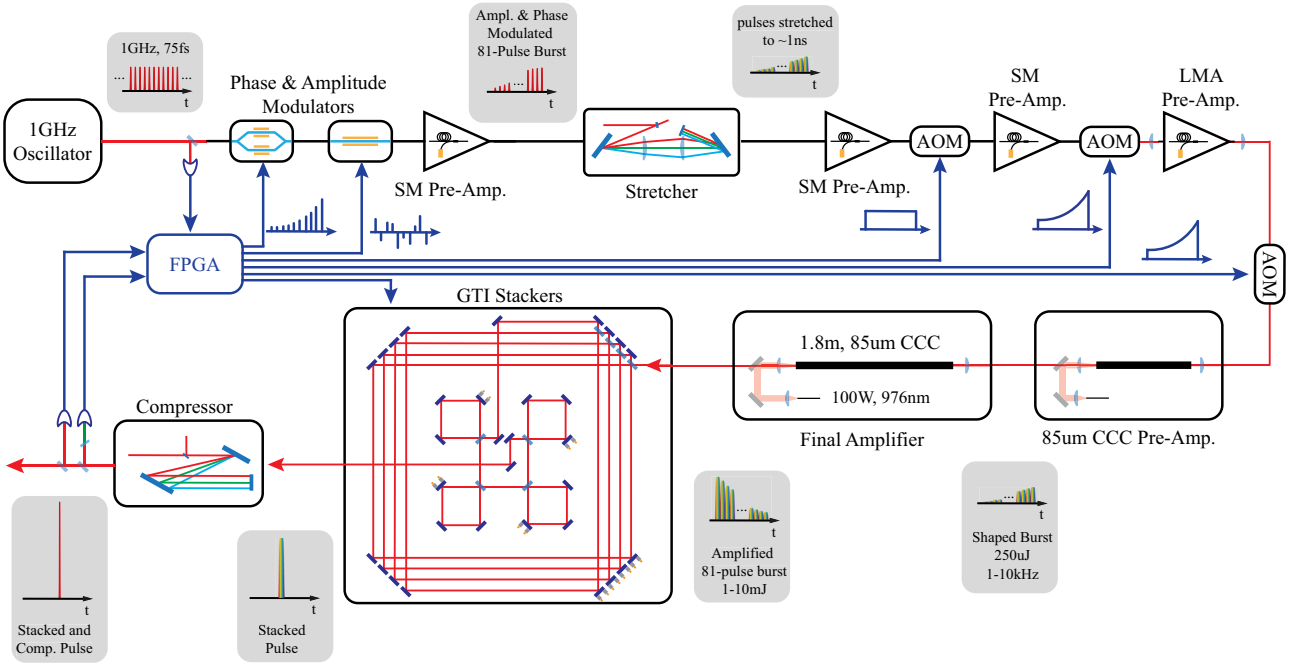

Fig. 5. Diagram of the CPSA demonstration system. Elements are shown connected with black lines to represent optical fiber or red lines to represent free-space beams. Control signals and connections are shown in blue; the gray insets show the evolution of the pulse bursts throughout the optical system.

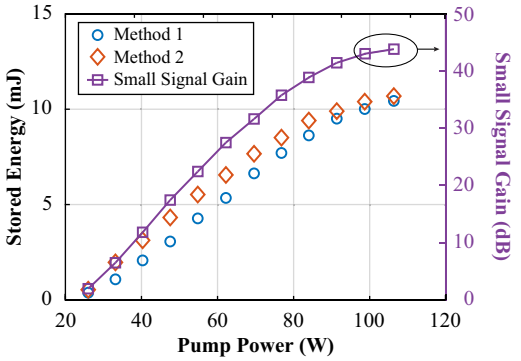

Fig. 6. Measurement of stored energy from 1.8 m of 85-μm-core CCC fiber using two different methods as described in Supplement 1. At 105 W of pump power, corresponding to $G_0 = 46$ dB, the stored energy is measured to be 10.6 mJ.

of high-efficiency multi-layer dielectric gratings in a double-pass configuration.

The measured stacking efficiency η_s can deviate from the theoretical efficiency due to errors in cavity alignment, stacking burst phase profile, and beam collimation, as well as due to beam distortions and uncompensated nonlinear phase accrual. Measurement of stacking efficiency requires resolving pulses separated by a nanosecond and is usually done using the compressed pulses incident on a fast photodiode, where the pulses are shorter than the photodiode response time. The measured peak voltage is directly proportional to the pulse energy; however, care must be taken to maintain a linear response over the whole dynamic range of the measurement.

An ideal GTI cavity has unity power transmission; however, in practice mirror coatings have some small losses. While the loss per cavity when using high-quality high-reflectivity (HR) coatings is negligible, the cumulative loss from eight GTI cavities, turning mirrors, and beamsplitter anti-reflection (AR) coatings can impact stacked pulse energy. These cumulative losses can be characterized by the throughput efficiency η_t, defined as the ratio of the output average power to the input average power of the stacker. The measured throughput efficiency of the 4 + 4 GTI stacker used in this work, in the configuration shown in Fig. 2(a), is measured to be $\eta_t = 90.5\%$, somewhat lower than the theoretical value of ∼96% expected for using R = 99.99% HR and R = 0.2% AR coatings. The stacked pulse energy is the product of the input burst energy, the stacking efficiency η_s, and the throughput efficiency η_t.

Each GTI cavity in the stacker must be actively stabilized to maintain its required round-trip phase ϕ_i against any phase drifts in the system in order to achieve stable stacking. For this each cavity has a mirror mounted on a piezo which is driven by a high-voltage amplifier controlled by a field-programmable gate array (FPGA). The FPGA is clocked off the 1 GHz fiber oscillator, providing 1GS/s ADC reads synchronous with the photodetector-measured stacked waveform and up to 5 GS/s DAC writes for controlling piezo and modulator (EOM and AOM) drivers. Simultaneous stabilization of all GTI phases is achieved by using a hill-climbing algorithm [usually a stochastic-parallel gradient descent (SPGD) variant], which maximizes the peak power of the stacked pulse, thus automatically finding and maintaining the correct ϕ_i values. Stabilization is initialized by finding the global maxima of the eight-parameter round-trip phase landscape of the stacker through a Lissajous scan [28,33]. The SPGD algorithm primarily compensates rapid phase drift from the mode-locked oscillator, as well as slow mechanical drift of the GTI cavities. Oscillator drift is minimized through RF locking the oscillator rep-rate to a rubidium frequency standard [26].

The stacking efficiency is first tested at low power using the signal from the last single-mode preamplifier, where the burst energy is 1 μJ. The amplifier saturation is negligible at this point, so an equal-amplitude truncated stacking burst is used, achieving stacking efficiency of up to 90%. The largest contribution to the difference from the theoretically expected 98% (see Fig. 2) is attributed to errors in the stacking-burst phase profile, due to its prescription being based solely on the theoretical stacker response. We anticipate that implementing real-time stacking-burst phase optimization in the experiment will further increase stacking efficiency. The SPGD algorithm maintains stabilization indefinitely (i.e., until it is stopped) with a stacked pulse peak power noise RMS of 0.7%, practically the same as that of unstacked pulses.

To test the effect of energy extraction and accrued nonlinear phase on stacking efficiency and pulse compression, the output

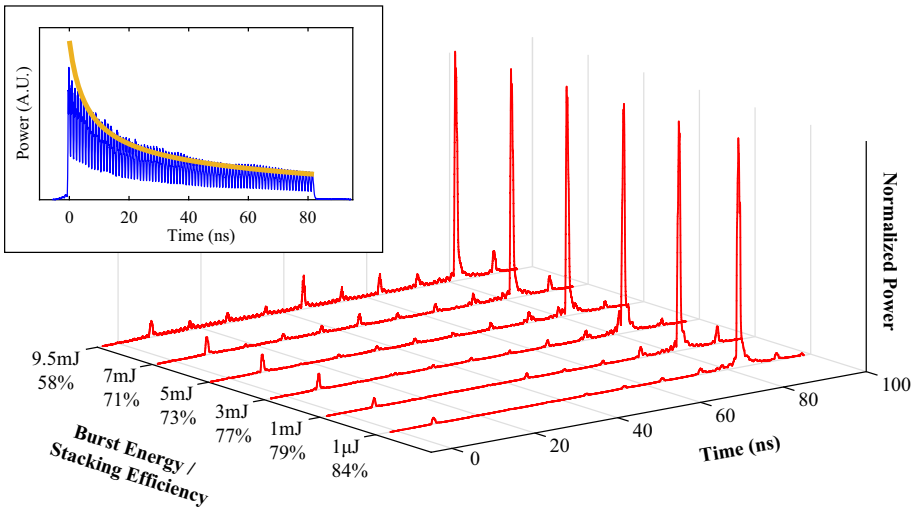

Fig. 7. Photodiode traces of the stacked pulses (red), including the low power result. The insert shows the 7 mJ stacking burst at the input of the stacker (blue) along with the calculated equal nonlinearity burst shape (yellow). The stacked traces are normalized to the peak of the stacked pulse and notated by the burst energy input to the stacker.

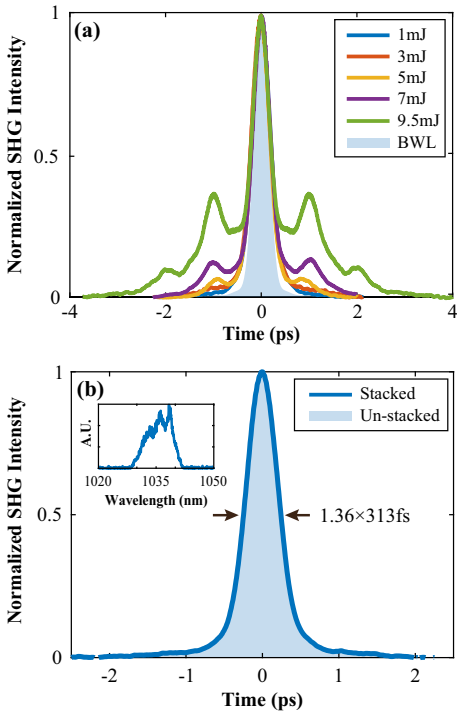

Fig. 8. Experimentally measured autocorrelation traces: (a) for final amplifier output energies from 1 mJ to 9.5 mJ and (b) comparison of stacked and unstacked traces at 3 mJ and spectrum at the output of the compressor (inset).

energy from the final amplifier is varied from 1 mJ to 9.5 mJ by increasing the pump power. At each output energy the amplified burst shape is matched to the calculated equal-nonlinearity burst shape for each corresponding degree of amplifier saturation by adjusting the electrical waveforms applied to the amplitude EOM and AOMs. The stacked pulses, as measured with a 22 GHz photodiode using 50 GHz sampling oscilloscope, are shown in Fig. 7, together with the 1 μJ result from the single-mode pre-amplifier.

The autocorrelation traces measured after stacking and compression for each indicated amplified burst energy are shown in Fig. 8(a). Comparison to the calculated bandwidth-limited (BWL) autocorrelation trace, represented as solid-filled blue, reveals that pulses at all energies have identical peak duration of 313 fs equal to this bandwidth limit. This is consistent with the low B-integral values anticipated from Fig. 3. This also indicates the absence of any detrimental effects due to stacking, further confirmed by the measured at 3mJ complete overlap between stacked and unstacked traces shown in Fig. 8(b).

However, there is a weak satellite pulse appearing in the autocorrelation trace at 5 mJ, which becomes very strong at 9.5 mJ. Although we initially attributed this to the onset of nonlinear effects, after careful further examination of our system we recognized that this was primarily caused by significant changes in the electrical waveform controlling the AOM right before the LMA preamplifier needed to compensate for increasingly high saturation of the final CCC stage at 5 mJ and 9.5 mJ. This caused some beam misalignment at the LMA stage input, leading to an in-burst varying excitation of a higher-order mode in this fiber. The satellite pulse appears due to a difference between fiber mode group velocities. This is confirmed by the observed onset of spectral beating (weak for 5 mJ and strong for 9.5 mJ), with the ∼3 nm period corresponding exactly to the 1.2 ps separation between the main and satellite pulse in the measured autocorrelation traces at these energies. Autocorrelation measurements are inherently symmetric, so the single satellite pulse appears on both sides of the trace. The existence of this higher-order mode produced satellite pulse explains why the structure on the autocorrelation traces in Fig. 8 is larger than is expected for the <4.5 rad of accrued nonlinear phase, according to Fig. 1(a). Note that due to the mode-filtering properties of CCC fibers, the single-mode beam quality from the final stage is not affected.

All stacked-waveform traces in Fig. 7 were obtained in the same experimental campaign; i.e., once the stacker alignment was completed, the beam from single-mode fiber pre-amplifier output was directed into it when measuring the 1 μJ trace, and the beam from 85 μm core CCC fiber power-amplifier output was directed into it when measuring mJ-scale traces. For this particular stacker alignment, optimized for high energies, the efficiency η_s at low energies was 84%. At high energies the highest stacking efficiency was 79% at 1 mJ, gradually decreasing with increasing energies to 71% at 7 mJ. Gradual decrease of approximately this magnitude is expected, according to Fig. 4. However, we attribute their overall lower efficiency compared to low energies (e.g. 79% at 1 mJ vesus 84% at 1 mJ) to larger errors in equal-nonlinearity stacking-burst profiles, stemming from their prescriptions being based on two theoretical-only models—the calculated stacker response and the numerical model of a saturated fiber amplifier. Furthermore, there is a rather rapid decrease in stacking efficiency down to 58% at 9.5 mJ, resulting in 4.2 mJ after compression. We attribute this primarily to the presence of satellite pulses (identified in the previously discussed autocorrelation traces) which constitute a separate satellite burst possessing a much lower stacking efficiency. A small contribution to reduced efficiency is from chirped pulse reshaping along the burst due to inversion-dependent gain spectrum in Yb-fiber amplifiers. We have confirmed that, for the 10 nm bandwidth stretched pulses used here, there are finite but small differences between the temporal shape of the first and last pulses in the 9.5 mJ waveform. This indicates that the effect on stacking efficiency is secondary and the monochromatic assumption in our equal-nonlinearity model is justified.

For future improvements, we plan to implement additional stacking-burst optimization loops, operating in real time in a running laser system, to correct any residual errors in the stacking-profile approximation using the numerical model. This should further improve stacking burst profile accuracy, and hence stacking efficiency, at both high and at low energies. At the highest ∼10 mJ energies, reduced compressed-pulse fidelity and lower stacking efficiency due to satellite pulses are expected to be resolved by replacing LMA stage with a single-mode preamplifier. If needed for further refinement, chirped pulse reshaping along the burst can also be compensated using a technique of in-burst spectral compensation with a 5 GHz amplitude EOM, reported in [34].

We had recently reported further energy scaling based on this CPSA technique by using coherent beam combining of four parallel fiber amplifiers to produce record high energies per fiber channel [35] and are in the process of further average power and energy scaling. We also used this CPSA system for initial high-intensity laser–matter experiments demonstrating the first fiber-laser based generation of neutrons, to the best of our knowledge [36].

5. CONCLUSIONS

In summary we have validated a new technique of coherent pulse stacking amplification of femtosecond pulses enabling a near-complete maximum stored energy extraction with low accumulated nonlinearity from a high-energy amplifier. The demonstrated extraction of up to 9.5 mJ in a 81-pulse stacking burst with the estimated accumulated B-integral of less than 4.5 rad, and the subsequent coherent pulse combining into a single pulse with its compression to 313 fs, represents, to our knowledge, the highest energy extracted and compressed to ultrashort duration from a single fiber amplifier. It constitutes nearly a two order of magnitude higher energy that is achievable with the same nonlinearity from such large-core fiber amplifier using only the CPA. We show that unique properties of coherent pulse stacking with GTI cavities enables efficient pulse combining with a strongly saturated pulse burst. We also show that there is an equal-nonlinearity profile, which minimizes and simultaneously equalizes accumulated nonlinearity for strong saturation. This validation of the CPSA technique enables a path to approximately two orders of magnitude size reduction of future high-energy coherently spatially combined fiber laser arrays.

The remaining challenge for the demonstrated CPSA technique is to eliminate residual pre-pulses in the stacked waveform, which are present due to incomplete destructive interference during coherent temporal combining. Although it has been shown theoretically that contrasts of $> 10^3$ might be achievable with coherent pulse stacking by using pre-burst optimization techniques [26], this would still fall significantly below what is required for the intended use of CPSA for driving high-intensity laser–matter interactions (e.g., pre-pulse contrasts of $> 10^5$ are needed for gas targets and $> 10^{10}$ for solid targets [6]). Just as in current TW-scale and PW-scale Ti:sapphire CPA systems, such high contrasts will only be achievable using external pulse "cleaning" techniques. Such a new pre-pulse cleaning technique, compatible with multi-J pulse energies and capable of 90%–95% efficiency when producing >50 dB contrasts in distortion-free beams, has been recently presented [37] and is currently pursued experimentally in our laser system.

Funding. U.S. Department of Energy (FP00013287).

Acknowledgment. The authors acknowledge John Nees for helpful discussions, nLight Inc for providing pump diodes, and Jay Dawson/Livermore National Lab for providing the compressor gratings.

Disclosures. The authors declare no conflicts of interest.

Data availability. Data underlying the results presented in this paper are not publicly available at this time but may be obtained from the authors upon reasonable request.

Supplemental document. See Supplement 1 for supporting content.

REFERENCES

1. F. Albert and A. G. Thomas, "Applications of laser wakefield accelerator-based light sources," Plasma Phys. Control. Fusion **58**, 103001 (2016).
2. A. Gonsalves, K. Nakamura, J. Daniels, *et al.*, "Petawatt laser guiding and electron beam acceleration to 8 GeV in a laser-heated capillary discharge waveguide," Phys. Rev. Lett. **122**, 084801 (2019).
3. R. Snavely, M. Key, S. Hatchett, *et al.*, "Intense high-energy proton beams from petawatt-laser irradiation of solids," Phys. Rev. Lett. **85**, 2945–2948 (2000).
4. J. Alvarez, J. Fernández-Tobias, K. Mima, *et al.*, "Laser driven neutron sources: characteristics, applications and prospects," Phys. Proc. **60**, 29–38 (2014).
5. H. Daido, M. Nishiuchi, and A. S. Pirozhkov, "Review of laser-driven ion sources and their applications," Rep. Prog. Phys. **75**, 056401 (2012).
6. "Report of the basic research needs workshop on laser technology," https://science.osti.gov/-/media/ardap/pdf/2024/Laser-Technology-Workshop-Report_20240105_final.pdf. Accessed: 2024-06-18.
7. A. Di Piazza, L. Willingale, and J. Zuegel, "Multi-petawatt physics prioritization (MP3) workshop report," arXiv (2022).
8. R. Falcone, F. Albert, F. Beg, *et al.*, "Workshop report: brightest light initiative (27-29 March 2019, OSA headquarters, Washington, DC)," arXiv (2020).
9. Y. Wang, H. Chi, C. Baumgarten, *et al.*, "1.1 J Yb:YAG picosecond laser at 1 kHZ repetition rate," Opt. Lett. **45**, 6615–6618 (2020).
10. E. F. Sistrunk, D. A. Alessi, A. J. Bayramian, *et al.*, "Laser technology development for high peak power lasers achieving kilowatt average power and beyond," Proc. SPIE **11034**, 1103407 (2019).
11. I. Fsaifes, L. Daniault, S. Bellanger, *et al.*, "Coherent beam combining of 61 femtosecond fiber amplifiers," Opt. Express **28**, 20152–20161 (2020).
12. E. A. Shcherbakov, V. V. Fomin, A. A. Abramov, *et al.*, "Industrial grade 100 kw power cw fiber laser," in *Advanced Solid-State Lasers Congress*, OSA, Paris, France, 2013, paper ATh4A.2.
13. "High power cw fiber lasers," https://www.ipgphotonics.com/en/products/lasers/high-power-cw-fiber-lasers#[1-micron]. Accessed: 2024-03-25.
14. T. Fan, "Laser beam combining for high-power, high-radiance sources," IEEE J. Sel. Top. Quantum Electron. **11**, 567–577 (2005).
15. S. J. McNaught, P. A. Thielen, L. N. Adams, *et al.*, "Scalable coherent combining of kilowatt fiber amplifiers into a 2.4-kW beam," IEEE J. Sel. Top. Quantum Electron. **20**, 174–181 (2014).
16. M. Müller, C. Aleshire, A. Klenke, *et al.*, "10.4 kW coherently combined ultrafast fiber laser," Opt. Lett. **45**, 3083–3086 (2020).
17. J. Limpert, F. Roser, D. N. Schimpf, *et al.*, "High repetition rate gigawatt peak power fiber laser systems: challenges, design, and experiment," IEEE J. Sel. Top. Quantum Electron. **15**, 159–169 (2009).
18. S. Webster, F. McDonald, A. Villanger, *et al.*, "Optical damage measurements for high peak power ytterbium doped fiber amplifiers," Proc. SPIE **5991**, 599115 (2005).
19. A. Galvanauskas, "Ultrashort-pulse fiber amplifiers," in *Ultrafast Lasers: Technology and Applications*, M. E. Fermann, A. Galvanauskas, and G. Sucha, eds. (CRC Press, 2002).
20. R. Lindberg, P. Zeil, M. Malmström, *et al.*, "Accurate modeling of high-repetition rate ultrashort pulse amplification in optical fibers," Sci. Rep. **6**, 34742 (2016).
21. T. Zhou, J. Ruppe, C. Zhu, *et al.*, "Coherent pulse stacking amplification using low-finesse Gires-Tournois interferometers," Opt. Express **23**, 7442–7462 (2015).
22. M. Chen, A. Rainville, M. Kanskar, *et al.*, "All-fiber integrated 85um core chirally-coupled core fiber high energy amplifiers for compact coherently combined laser arrays," Proc. SPIE **12400**, 124000I (2023).
23. M. Kienel, A. Klenke, T. Eidam, *et al.*, "Energy scaling of femtosecond amplifiers using actively controlled divided-pulse amplification," Opt. Lett. **39**, 1049–1052 (2014).
24. H. Stark, M. Müller, M. Kienel, *et al.*, "Electro-optically controlled divided-pulse amplification," Opt. Express **25**, 13494–13503 (2017).
25. H. Stark, M. Benner, J. Buldt, *et al.*, "Pulses of 32 mJ and 158 fs at 20-kHZ repetition rate from a spatiotemporally combined fiber laser system," Opt. Lett. **48**, 3007–3010 (2023).
26. M. Whittlesey, "Advanced techniques for spectral & temporal ultrashort pulse synthesis in coherent pulse stacking amplification," Ph.D. thesis (University of Michigan, 2022).
27. F. Gires, "Interferometer utilisable pour la compression d'impulsions lumineuses modulees en frequence," C. R. Acad. Sci. **258**, 6112 (1964).
28. J. M. Ruppe, "Theoretical and experimental foundations of coherent pulse stacking amplification," Ph.D. thesis (University of Michigan, 2017).
29. L. M. Frantz and J. S. Nodvik, "Theory of pulse propagation in a laser amplifier," J. Appl. Phys. **34**, 2346–2349 (1963).
30. R. Paschotta, J. Nilsson, A. Tropper, *et al.*, "Ytterbium-doped fiber amplifiers," IEEE J. Quantum Electron. **33**, 1049–1056 (1997).
31. Y. Sintov, O. Katz, Y. Glick, *et al.*, "Extractable energy from ytterbium-doped high-energy pulsed fiber amplifiers and lasers," J. Opt. Soc. Am. B **23**, 218–230 (2006).

32. C. Li, Y. Ma, X. Gao, *et al.*, "1 GHz repetition rate femtosecond Yb:fiber laser for direct generation of carrier-envelope offset frequency," Appl. Opt. **54**, 8350–8353 (2015).
33. H. Pei, "High fidelity coherent pulse stacking amplification with intelligent system controls," Ph.D. thesis (University of Michigan, 2021).
34. S. Chen, "Spectral and temporal control of broadband pulses to enable multi-tw peak power coherently-combined fiber laser arrays," Ph.D. thesis (University of Michigan, 2021).
35. A. Rainville, M. Whittlesey, C. Pasquale, *et al.*, "Stable and efficient coherent pulse stacking amplification of 81 pulses with four channel coherent spatial combining at 7 mJ/fiber," in *CLEO* (Optica, 2023), paper SF3H.6.
36. C. Pasquale, A. Rainville, N. Peskosky, *et al.*, "Fast neutron generation from ultrafast spatially and temporally coherently combined fiber laser driver," in *APS Division of Plasma Physics Meeting Abstracts*, Vol. 2023 of APS Meeting Abstracts (2023), p. CO08.009.
37. M. Garner, T. Coleman, A. Rainville, *et al.*, "Multi-joule scalable, distortion-free pre-pulse contrast enhancement using multi-pass cells," in *Advanced Accelerator Concepts Workshop* (2024).